The Study of Time Constant Analysis in Random Telegraph Noise at the Subthreshold Voltage Region

A. Yonezawa[1], A. Teramoto[2], T. Obara[1] , R. Kuroda[1], S. Sugawa[1,2], and T. Ohmi[2]
1 Graduate School of Engineering, 2 New Industry Creation Hatchery Center
Tohoku University,
Sendai, Japan
Phone: +81-22-795-3977 E-mail: yonezawa@fff.niche.tohoku.ac.jp

***Abstract*—We extracted time constants capture and emission of Random Telegraph Noise (RTN), and their dependencies of the gate-source voltage from numerous MOSFETs and discuss the trapping and detrapping processes of carriers at the subthreshold voltage region. The dependence of time to capture on gate-source voltage cannot be determined by the trap depth from the interface and but by the distance between the trap and the carrier to be captured and the trap energy level. On the other hand, it is considered that the dependence of time to emission is determined by the distance between the trap and the Si/SiO$_2$ interface and the trap energy level. It is easy to understand emission processes compared to capture processes. We observed various emission processes caused by tunneling to Si substrate side, tunneling to gate electrode side and tunneling to either Si substrate side or gate electrode side depending on gate-source voltage.**

Evaluating the time constants individually is indispensable to characterize the trap which causes RTN in subthreshold voltage region.

Keywords-component; MOSFET, Random Telegraph Noise (RTN), Subthreshold Voltage, Time Constant

I. Introduction

Random Telegraph Noise (RTN) has been believed as one of the physical origins of low frequency noise. The phenomenon is characterized by a discrete and random fluctuation of conductance in carrier transport and the number of conduction carriers, which is caused by the capture/emission of the conduction carrier by/from individual traps in an insulator film or bulk material [1].

Recently, the impacts of RTN on the MOSFETs have become larger as the progression of CMOS circuit scaling down continues. It is known that RTN amplitude is greater as the number of channel carriers decreases. The channel carrier density (Q_{ch}) is very small in the subthreshold region, and then RTN becomes very large even in the relatively large MOSFETs. Especially, the in-pixel source-follower transistors in CMOS image sensors are operated in near the subthreshold voltage region. RTN causes image quality degradation of CMOS image sensors [2, 3]. Consequently, a reduction of RTN is strongly required.

The amplitude and the time constants including the time to capture and the time to emission (τ_c and τ_e) are important parameters of RTN characteristics. An accurate evaluation at these parameters is indispensable for an understanding of the mechanism of RTN. In this paper, we extracted τ_c and τ_e accurately in the subthreshold region and based on the experimental data of fabricated MOSFETs, we discuss about models of capture and emission processes with the traps which cause RTN.

II. Experimental

The analysis of RTN requires a measuring numerous MOSFETs because the RTN characteristics: τ_c, τ_e and amplitude, have large variation by the variation of the trap properties: energy level and special location and the variation of channel caused by the non-uniformity effect [4]. We employed the arrayed test circuit to detect and analyze RTN statistically from numerous MOSFETs in a short time [5, 6]. Fig.1 shows (a) Measurement system (b) the arrayed test circuit diagram. Measured MOSFETs are placed in an array, and a short time measurement is carried out by reading the output

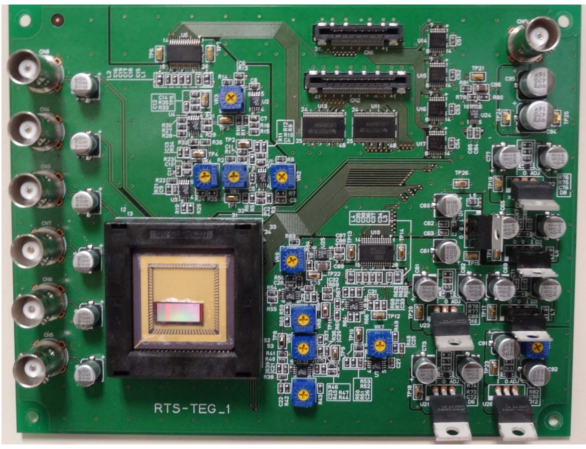

(a) Measurement system

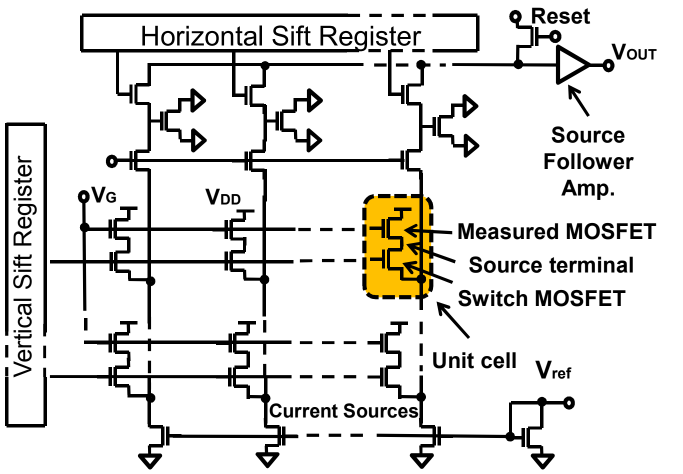

(b) Arrayed test circuit diagram.
Figure 1.Measureement system

voltage (V_{out}), while a constant drain current is applied. RTN appears as the voltage fluctuation of the output voltage which is the source terminal voltage of the measured MOSFET. The test circuit was fabricated by the standard 0.22 μm CMOS technology. The gate oxide thickness (T_{ox}), the gate length and the gate width of MOSFETs were 5.7 nm, 0.22 μm and 0.28 μm, respectively. 131072-MOSFETs were arrayed in the test pattern. Fig.2 shows the measurement sequence. To detect MOSFETs with RTN, a root mean square of V_{out} in time domain (V_{rms}) were extracted with the sampling period of 0.7 s and record time of 600 s [5, 6].

We extracted MOSFETs of which V_{rms} were greater than 680 μV. 8215-MOSFETs were extracted. Then, 137-MOSFETs were selected randomly for analyzing RTN characteristics by the high frequency sampling measurements. The RTN parameters of τ_c, τ_e and the amplitude were extracted accurately with sampling period of 1 μs and record time of 600 s (6×10^8 points) and set the same back bias (V_{bs}) of -1.2 V was applied for every MOSFET. The back bias difference caused by threshold voltage (V_{th}) variation was eliminated. For the simplicity of analysis, we removed RTN with more than two states after high frequency sampling (109 / 137 MOSFET). In this experiment we discuss the RTN time constants of twenty-eight MOSFETs with two states RTN.

Fig. 3 shows the method of RTN parameter extraction from the V_{gs}-time data [7]. Average values of τ_c and τ_e ($\langle\tau_c\rangle$ and $\langle\tau_e\rangle$) were extracted by fitting the distribution of extracted τ_c and τ_e using (1), assuming these phenomena follow the Poisson process [1].

$$\mathrm{Counts}(\tau_{c,e}) = \mathrm{A}\exp\left(-\frac{\tau_{c,e}}{\langle\tau_{c,e}\rangle}\right) \quad (1)$$

where A is a constant.

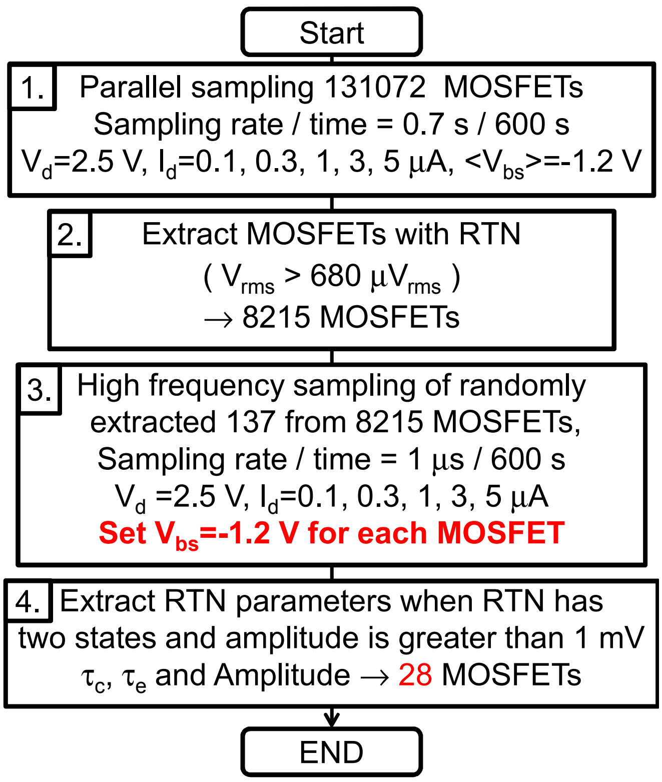

Figure 2. Measurement sequence

III. Results and Discussions

Fig.4 shows the cumulative probability of V_{rms} in Gumbel plot for five drain currents (I_d). V_{rms} value increase as the decrease of I_d. It is because the screening effect of the potential burrier of the trapped charge becomes greater as the decrease of the number of the channel carriers [8].

Fig.5 shows the band diagram for the energy changing of trap in the oxide when V_{gs} changes. Assuming the trap energy level does not change as V_{gs} changes, E_t follows (2).

$$\Delta(E_t - E_c) = \frac{X \cdot \Delta V_{ox}}{T_{ox}} \quad (2)$$

The E_c and V_{ox} are the lowest energy of conduction band and applied oxide voltage. Assuming the distance between the trap and the electron to be captured is the same as X, and electrons are captured/emission of the conduction carrier by/from the inversion layer. The tunneling probability of the electron in channel to the trap and that of from the trap to the conduction band decreases and increases with V_{ox} increasing respectively. As a result, it is considered that τ_c decreases and τ_e increases with the increase of V_{gs}.

Fig.6 show the time constants as a function of V_{gs} for (a) τ_e and (b) τ_c. In Fig.6 (a), almost all τ_e increase as the increase of V_{gs}. On the contrary, τ_c decrease with V_{gs} increase for all samples. The slopes of τ_c are much larger than those of τ_e. When carrier is captured by the tunnel effect, the τ_c follows (3).

$$\tau_c = \frac{1}{v_n \sigma_n Q_{ch}} \exp\left(\frac{E_t - E_c}{kT}\right) \quad (3)$$

Where v_n, σ_n, k and T are thermal velocity, capture cross-section, Boltzmann constant and temperature, respectively. And then, τ_c depends on the potential barrier from the channel to the trap and the number of channel carriers. Fig.7 shows the ($\tau_c \times I_d$) as a function of V_{gs}. τ_c are normalized by Q_{ch}, assuming I_d is proportional to Q_{ch}. By normalizing by Q_{ch}, ($\tau_c \times I_d$) is related the tunneling probability for one electron. For example (A) and (B), ($\tau_c \times I_d$) of the some samples decrease in the increase of V_{gs}

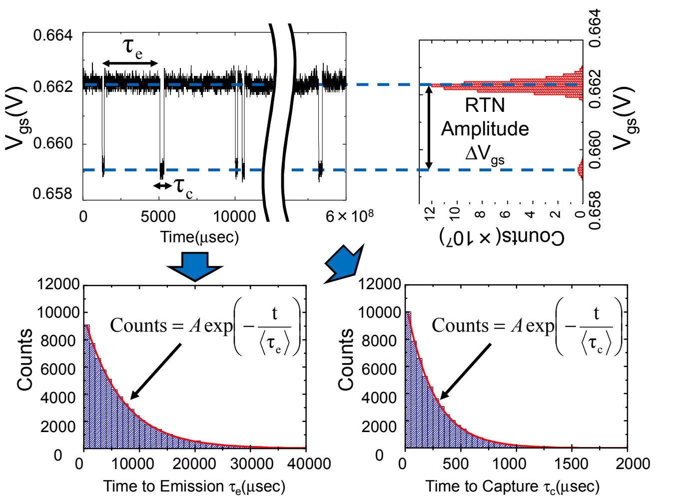

Figure 3. Definitions and extraction methods of $\langle\tau_c\rangle$, $\langle\tau_e\rangle$ and amplitude from RTN waveform data [7].

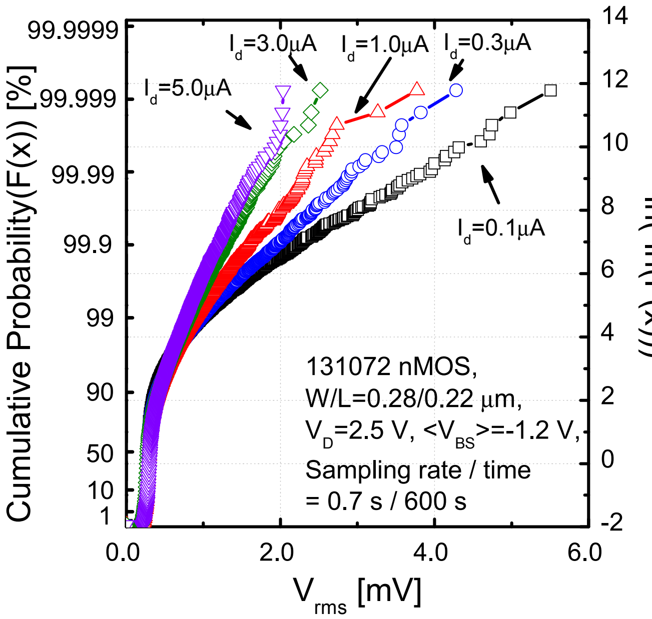

Figure 4. Cumulative probability of V_{rms} for five drain currents.

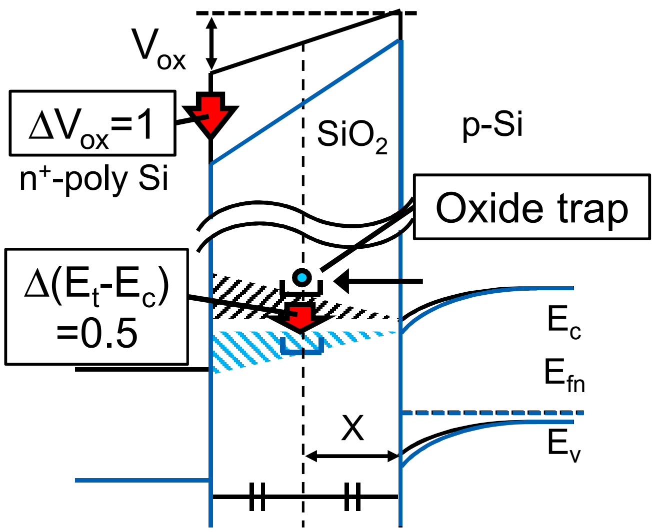

Figure 5. Band diagram of the trap energy changing as V_{gs} increasing.

and there is great variation among the slope of (τ_c x I_d). On the contrary, for example (C), (τ_c x I_d) of the 10 samples increase with an increase of V_{gs}. These characteristics of (C) are very complicated and cannot be explained if the distance of trap and a carrier to be captured is the same as the trap depth. Fig.8 shows (a) 3D and (b) cross-sectional schematic views of locations of the trap and the channel of the type same as (C) in Fig.7. The carrier is captured from percolation path [4]. The percolation path is formed at the Si interface from the source to the drain locally, and then the distance between the trap and the electron to be captured is not the depth of trap (X), and the carrier number in the percolation path is not defined as Q_{ch}. It is considered that the distance between the percolation path and the trap become longer as the increase of V_{gs}.

On the other hand, the emission is considered to be determined from the trap to the nearest state of either the Si substrate conduction band of Si substrate or the gate electrode regardless of the percolation path in Si substrate because there are the empty states in the conduction band exist in the silicon

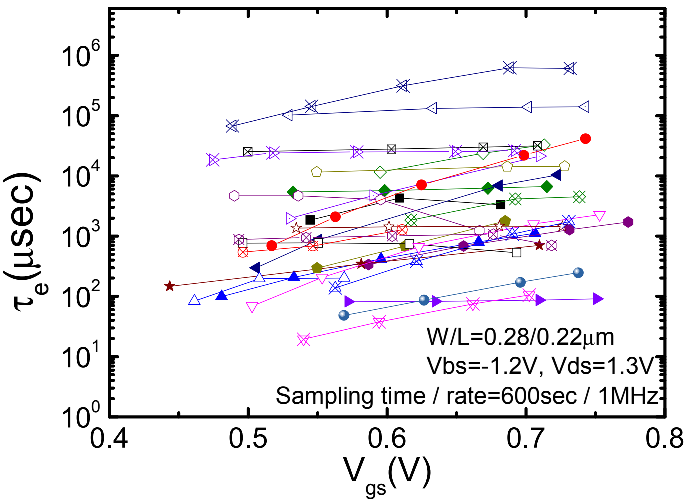

(a) Slopes of τ_e vs. V_{gs}

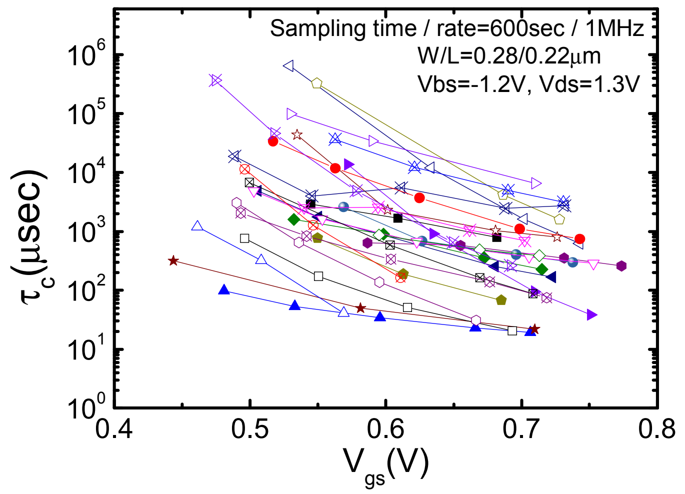

(b) Slopes of τ_c vs. V_{gs}

Figure 6. Time constants as a function of V_{gs} for (a) τ_e and (b) τ_c.

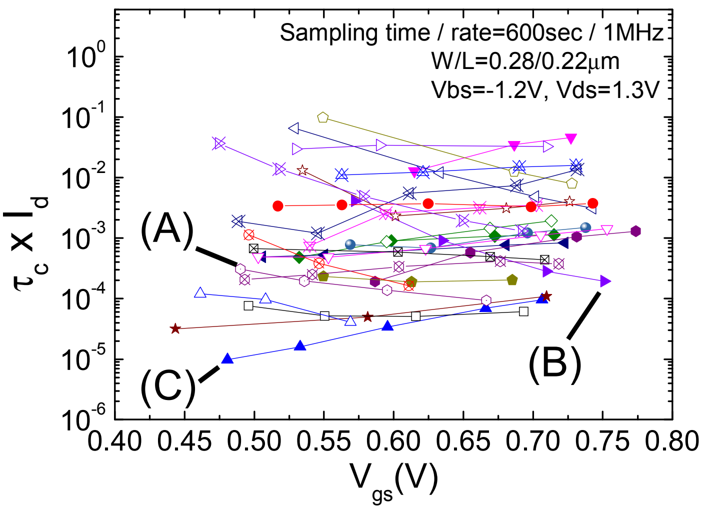

Figure 7. Normalized τ_c (I_d x τ_c) as a function of V_{gs}
By normalizing by Q_{ch}, (τ_c x I_d) is related the tunneling probability for one electron.

surface. As mentioned above, the dependence of V_{gs} on τ_c becomes complicated. When percolation paths are formed, and the number of trapped electron is one, it is considered that tunneling probability depends on only E_t, X, and V_{gs}.

We classified the obtained dependencies of τ_e on V_{gs} into three

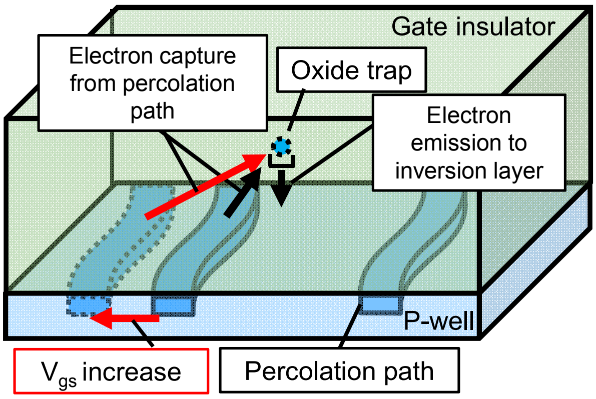

(a) 3D schematic view of the trapping and detrapping model.

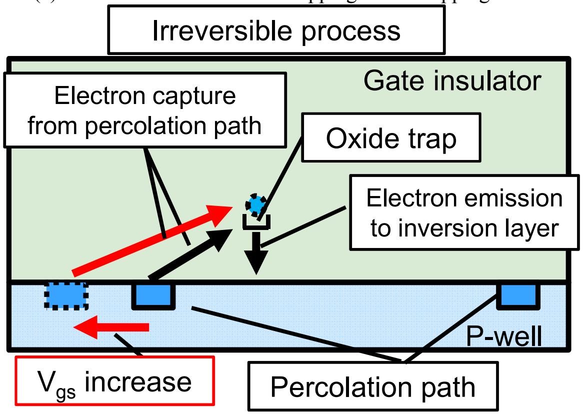

(b) Cross-section of the trapping and detrapping model.
Figure 8. 3D schematic and cross-section views of the trapping and detrapping model.

categories as explained below. In Fig 9-11, (a) τ_e as the function of V_{gs} (b) RTN wave forms of typical (c) band diagram with trapping and detrapping process respectively for each category.

In category 1, τ_e monotonically increases as the increase of V_{gs} as shown in Fig.9 (a). In Fig.9 (b), the amplitude becomes smaller and τ_c becomes shorter with the increase of V_{gs} (I_d).As shown in Fig.9 (b), (D) has two states RTN; these indicate that RTN of sample (D) is confirmed to be caused by one trap. It is considered that the tunneling probability decrease with an increase of V_{gs} and this indicates that the direction of emission is from the trap to the Si substrate side as shown in Fig.9(c).

In category 2, τ_e monotonically decreases as the increase of V_{gs} as shown in Fig.10 (a). In Fig.10 (b), the amplitude becomes smaller, τ_c becomes shorter with the increase of V_{gs} (I_d) respectively. Then, these indicate that the RTN of sample (E) is defined to be caused by one trap. It is considered that tunneling probability increases with an increase of V_{gs} and the direction of emission is from the trap to the gate electrode side. In this case, the trapped carrier is emitted to the gate electrode side though the electron is captured from the Si substrate side to the trap, then the processes in category 2 are irreversible process as shown in Fig 10 (c).

In category 3, τ_e increases with the increase of V_{gs} at small V_{gs} region, however τ_e decreases with the increase of V_{gs} at a large V_{gs} region as shown in Fig.11 (a). In Fig.11 (b), RTN amplitude monotonically decreases with the increase of V_{gs} and τ_c decreases with the increase of V_{gs} (I_d), monotonically. It is

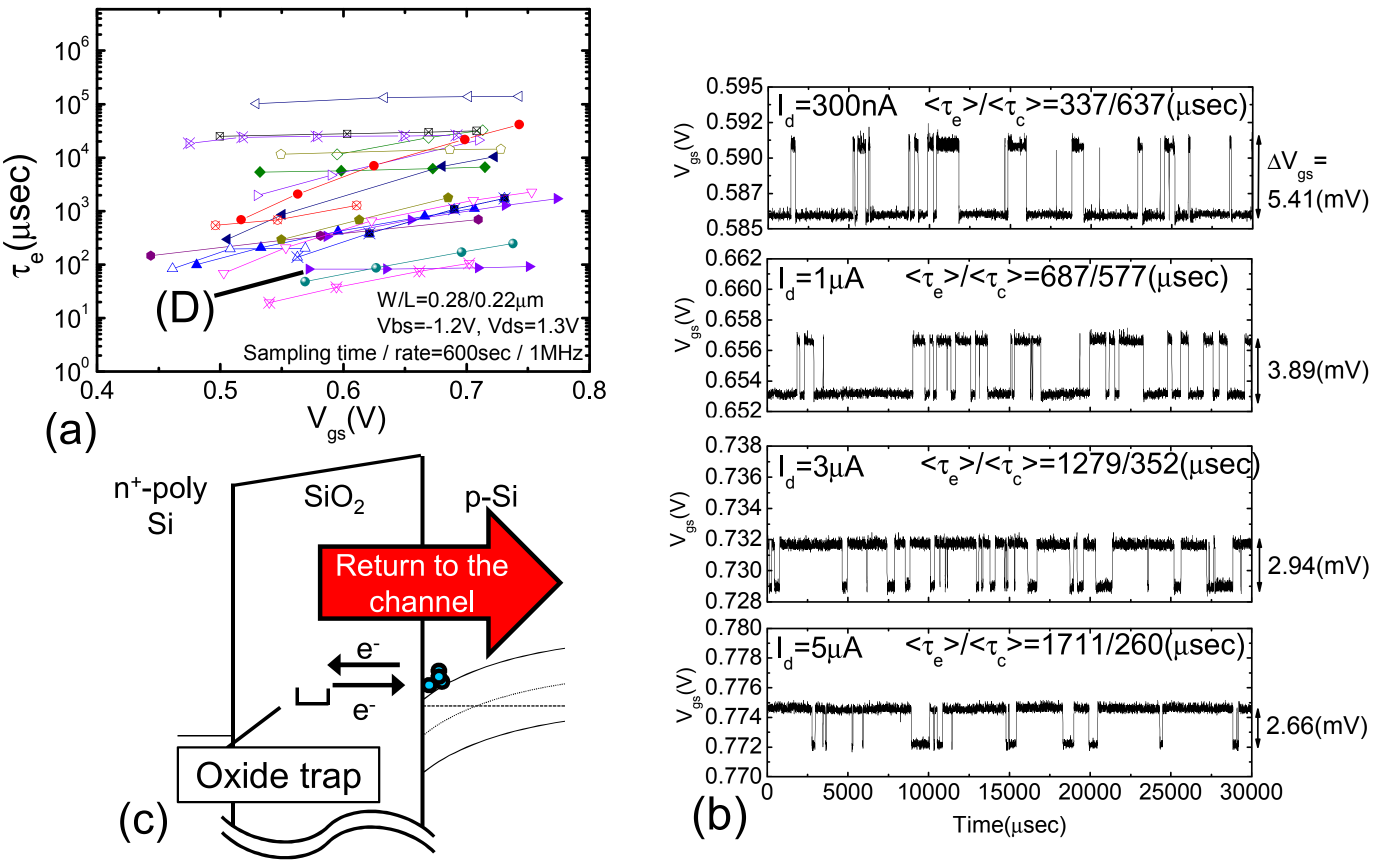

Figure 9. The measurement data and trap-detrap model of category 1 (τ_e monotone increasing).
(a) τ_e as the function of V_{gs}, (b) RTN waveform I_d= 0.3 ~ 5μ A, (c) Trap-detrap model

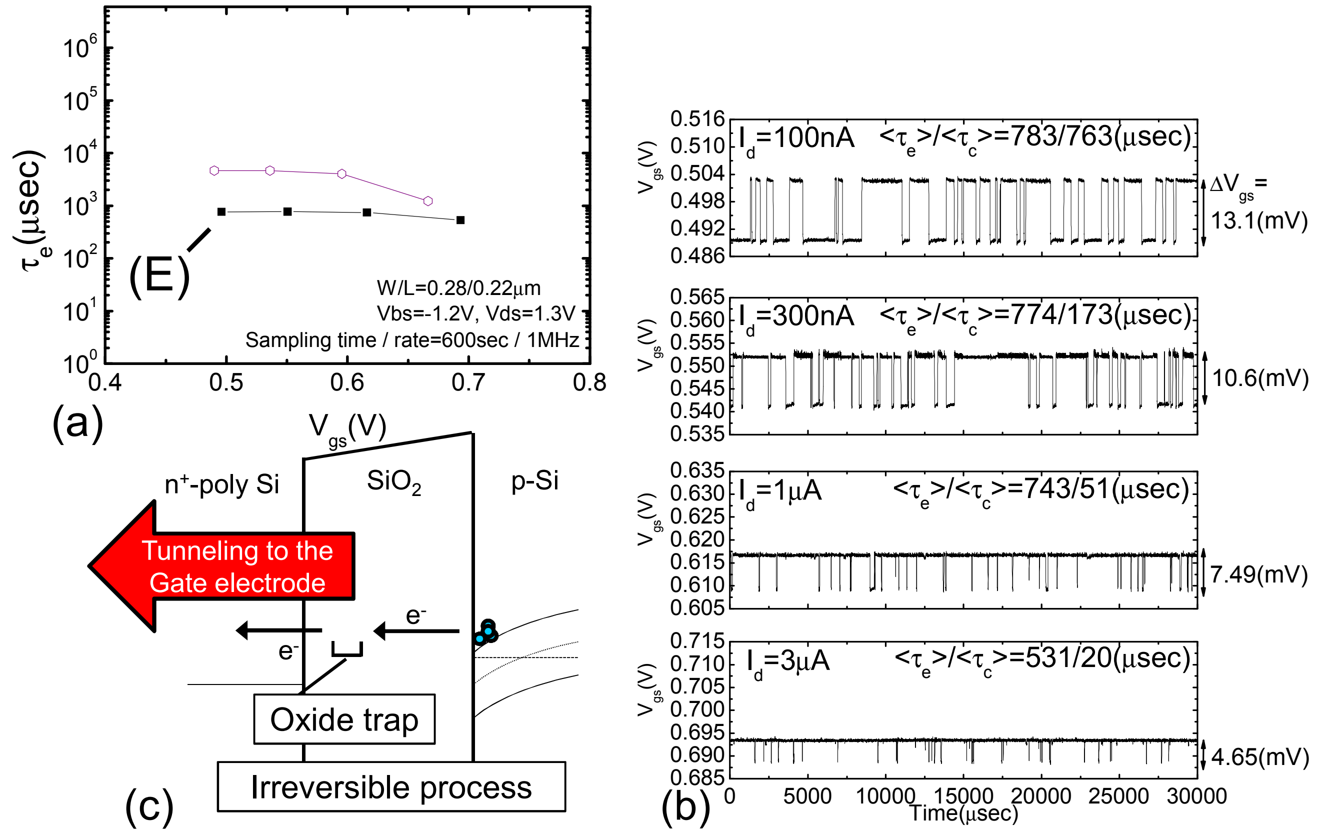

Figure 10. The measurement data and trap-detrap model of category 2 (τ_e monotone decreasing).
(a) τ_e as the function of V_{gs}, (b) RTN waveform I_d= 0.1 ~ 3µ A, (c) Trap-detrap model

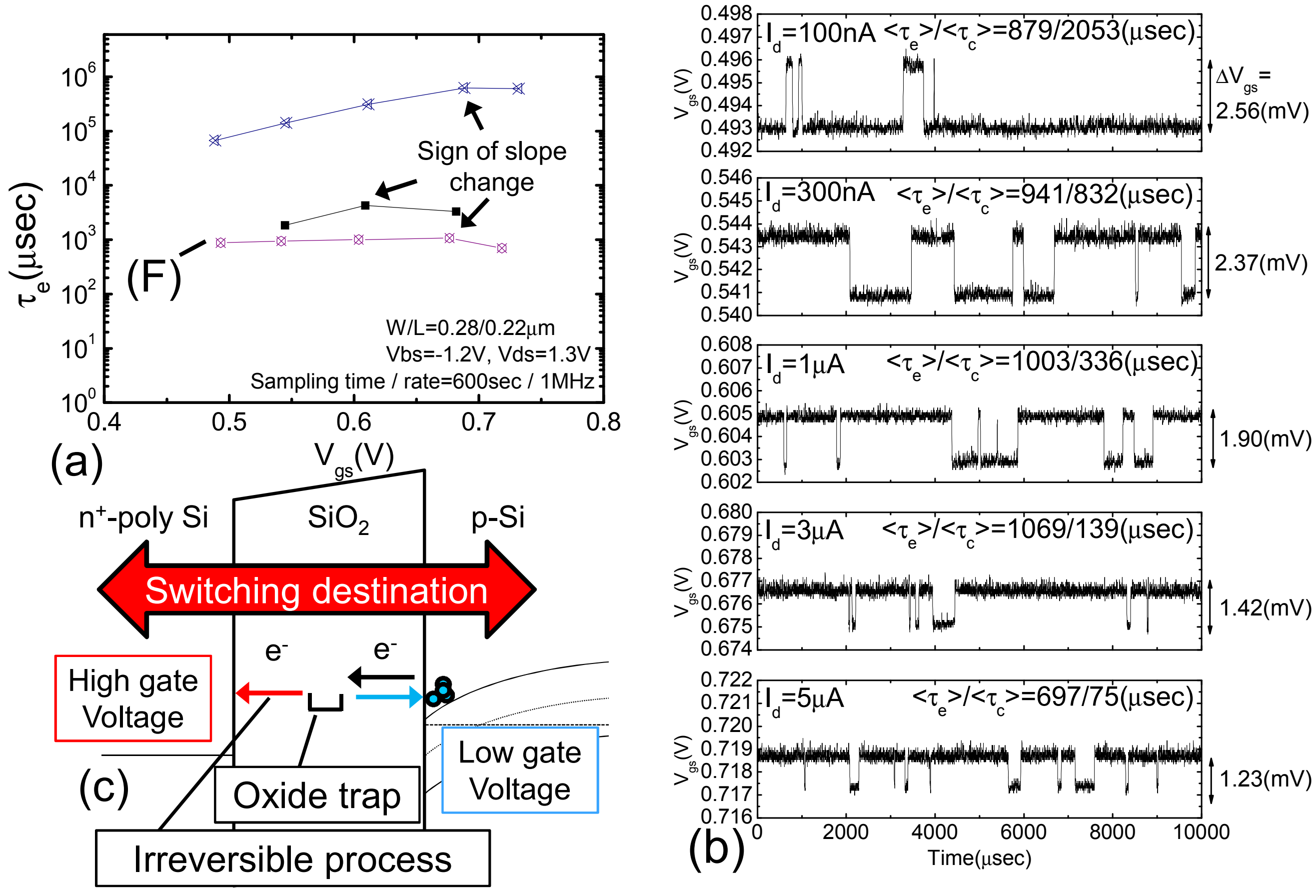

Figure 11. The measurement data and trap-detrap model of category 3 (the slope of τe with regards to V_{gs} changes).
(a) τ_e as the function of V_{gs}, (b) RTN waveform I_d= 0.1 ~ 5µ A, (c) Trap-detrap model

considered that the RTN of the sample (F) is caused by one trap. The tunneling probability dependence on V_{gs} changes at V_{gs} of 0.68 V. When small V_{gs} is applied, the trapped carrier is emitted to the Si substrate side, on the contrary when large V_{gs} is applied, the tunneling probability to the gate electrode side becomes larger than that to the Si substrate side. In this case as shown in Fig.11 (c), the trapped carrier is emitted to Si substrate side at the small V_{gs} region and to gate electrode side at the large V_{gs} region. When the trapped carrier is emitted to the gate electrode side, the process in category 3 is irreversible process.

IV. CONCLUSION

We extracted the various time constants of RTN and their dependence on V_{gs} and then proposed some trapping and detrapping to explain the experimental data of fabricated MOSFET. In our measurement the dependence of τ_c on V_{gs} cannot be determined by the trap depth from the interface but by the distance between the trap and the carrier to be captured and the trap energy level. On the contrary, since time to emission is mainly determined by the V_{gs}. It is easy to understand emission processes compared to capture processes. We observed various emission processes caused by tunneling to Si substrate side, tunneling to gate electrode side and tunneling to either Si substrate side or gate electrode side depending on V_{gs}. Some of these categories are irreversible process and it is considered that these phenomena hardly follow Shockley-Read-Hall statistics [1, 9].

Evaluating the τ_c and τ_e individually is indispensable to characterize the RTN trap in subthreshold region of MOSFET operation.

ACKNOWLEDGMENT

We would like to thank Mr. Y. Kamata and Mr. K. Shibusawa for sample fabrication and useful discussions.

REFERENCE

[1] M. J. Kirton and M. J. Uren, "Noise in solid-state microstructures: A new perspective on individual defects, interface states and low-frequency (1/f) noise," Adv. Phys., vol. 38, pp. 367-468, 1989.

[2] C. Leyris, F. Martinez, M. Valenza, A. Hoffmann, J. C. Vildeuil, and F. Roy, "Impact of Random Telegraph Signal in CMOS Image Sensors for Low-Light Levels," Proc. 32nd European Solid-State Circuits Conf., Montreux, pp. 376-379, 2006.

[3] X. Wang, P. R. Rao, A. Mierop, and A. J. P. Theuwissen, "Random Telegraph Signal in CMOS Image Sensor Pixels," Int. Electron Devices Meeting, San Francisco, pp. 115-118, 2006.

[4] A. Asenov, R. Balasubramaniam, A. R. Brown, and J. H. Davies, "RTS amplitudes in decananometer MOSFETs: 3-D simulation study," IEEE Trans. Electron Devices, vol. 50, pp. 839-845, 2003.

[5] S. Watabe, S. Sugawa, A. Teramoto, and T. Ohmi, "New Statistical Evaluation Method for the Variation of Metal-Oxide-Semiconductor Field-Effect Transistors," Japanese Journal of Applied Physics, vol. 46, pp. 2054-2057, Apr. 2007.

[6] K. Abe, S. Sugawa, S. Watabe, N. Miyamoto, A. Teramoto, Y. Kamata, K. Shibusawa, M. Toita, and T. Ohmi, "Random Telegraph Signal Statistical Analysis using a Very Large-scale Array TEG with 1M MOSFETs," IEEE Symp. VLSI Technol., Kyoto, pp. 210-211, 2007.

[7] K. Abe, A.Teramoto, S.Sugawa; T.Ohmi, "Understanding of traps causing random telegraph noise based on experimentally extracted time constants and amplitude" IRPS, 2011

[8] K. Abe, S. Sugawa, R. Kuroda, S Watabe, N. Miyamoto, A Teramoto, et al.: "Analysis of Source Follower Random Telegraph Signal Using nMOS and pMOS Array TEG", in Proc. Int. Image Sensors Workshop, pp.62-65, 2007

[9] W. Shockley and W. T. Read, "Statistics of the Recombination of Hole and electrons" Physical Review, vol87, no. 5, p.835-842, 1952